Charge-charge correlation functions in the Emery three-band model

Kupčić, Ivan

Source / Izvornik: **Physical review B: Condensed matter and materials physics, 2000, 61, 6994 - 7004**

Journal article, Published version
Rad u časopisu, Objavljena verzija rada (izdavačev PDF)

https://doi.org/10.1103/PhysRevB.61.6994

Permanent link / Trajna poveznica: https://urn.nsk.hr/urn:nbn:hr:217:099601

Charge-charge correlation functions in the Emery three-band model

Ivan Kupčić
Department of Physics, Faculty of Science, University of Zagreb, HR-10001 Zagreb, Croatia
(Received 13 July 1999; revised manuscript received 17 November 1999)

The influence of the long-range Coulomb forces on the charge-charge correlation functions has been examined in the Emery three-band model. The $U_d=0$ limit and the mean-field approximation of the $U_d\to\infty$ limit have been studied. The intraband and interband contributions to the dynamically screened correlation functions are found both for the intercell (monopole) and intracell (quadrupole) charge fluctuations. It appears that the interband monopole processes are responsible for the optical interband transitions. For strong local correlations ($U_d\to\infty$), the threshold energy of these processes is found to be only slightly dependent on the bare hybridization parameter t_{pd}^0/Δ_{pd}^0. The value of the threshold energy is comparable with the bare first-neighbor overlap energy t_{pd}^0. As expected from experimental observations and previous static, symmetry-based theoretical considerations, the oxygen-oxygen charge correlation function is not screened in the tetragonal lattices, in contrast to the oxygen-copper (pd) charge correlation function. The intraband coupling of the Raman-active phonons to the pd intracell charge fluctuations becomes thus substantially screened, but does not vanish, at variance with the predictions of the static-screening models. It is also found that the mean-field approximation of the $U_d\to\infty$ case can explain the measured magnitude of the plasma frequency, as well as its dependence on doping, but only in the overdoped high-T_c superconductors.

I. INTRODUCTION

In numerous high-T_c compounds a considerable amount of data related to the dielectric function $\varepsilon(\mathbf{Q},\omega)$ has been collected during the past decade.[1–7] The optical-conductivity measurements provide various information, such as the ω dependence in the Drude regime, the doping dependence of the plasma frequency, and the material dependence of the interband absorption edge. Similarly, in the Raman experiments the electronic and ionic charge fluctuations are probed. The corresponding phonon self-energies, the electron-phonon coupling constants, and the intracell charge-charge correlation functions will be screened by $\varepsilon(\mathbf{Q},\omega)$, more or less, according to their symmetries.

The theoretical analyses of these data assume usually reduced models suitable for the explanation of particular problems.[8–13] Our purpose here is to construct a more complete (but still approximate) response theory of the three-band model, to find the screened charge-charge correlation functions, and to check the results against the experimental data. The most important questions, which the simplified models fail to explain, are as follows. (i) The structure of the interband processes as a function of the three-band-model parameters. (ii) The dynamic screening of the intracell charge-charge correlation functions at the optical-phonon frequencies, in particular in the A_{1g} channel. (iii) The influence of the strong local correlations on the copper ions on both the optical conductivity and Raman spectra. However, our results will be limited by the use of several approximations: (i) To simplify calculations we study the response of the interacting electrons to the external longitudinal long-wavelength fields. In this way, the *longitudinal* dielectric function and the associated charge-vertex functions will be determined. (ii) Another simplification is made by not considering the short-range Coulomb interactions. (iii) Finally, the scattering of electrons on impurities and phonons is taken into account only phenomenologically.

The paper is organized as follows. In Sec. II we analyze the response of the interacting electrons to the external fields. The intracell charge fluctuations are symmetrized according to the space-group symmetry of the tetragonal lattice, and then the dielectric function is determined by using the corresponding matrix representation of the random-phase approximation (RPA). The screened charge-charge correlation functions are found and discussed in some detail.

In Sec. III we compare the obtained results with the experimental observations. First, we reexamine the problem of how the coupling between the electrons and the Raman-active phonons will be screened by the long-range forces in $YBa_2Cu_3O_{7-x}$. Then, the Drude and interband contributions to the optical conductivity as well as the doping dependence of the plasma frequencies are discussed in the context of the strong local correlations on the copper ions. Concluding remarks are given in Sec. IV.

II. THEORETICAL ANALYSIS

A. Three-band model

We consider a response of the interacting holes (the hole picture will be used) to the external scalar fields. It will be assumed that, besides the local Hubbard interaction on the copper ions U_d, only the long-range Coulomb interactions are present. The Hamiltonian is of the form

$$H=\mathcal{H}_0+H^{\mathrm{c}}+H^{\mathrm{ext}}. \tag{1}$$

Here $\mathcal{H}_0$ is the three-dimensional (3D) bare Hamiltonian:[14]

$$\begin{aligned}\mathcal{H}_0=&\sum_{N\sigma}\left[E_d^0 d_{N\sigma}^\dagger d_{N\sigma}+E_p^0(p_{xN\sigma}^\dagger p_{xN\sigma}+p_{yN\sigma}^\dagger p_{yN\sigma})\right]\\&+\sum_{N\sigma}t_{pd}^0[(p_{xN\sigma}^\dagger+p_{yN\sigma}^\dagger)d_{N\sigma}\\&-(p_{xN-a\sigma}^\dagger+p_{yN-b\sigma}^\dagger)d_{N\sigma}+\mathrm{H.c.}]\\&+\sum_N U_d d_{N\uparrow}^\dagger d_{N\uparrow}d_{N\downarrow}^\dagger d_{N\downarrow},\end{aligned} \tag{2}$$

H^{c} is the interaction Hamiltonian which describes the long-range forces among the intercell (monopole) charge fluctuations:

$$H^{c}\approx\frac{1}{2}\sum_{NN'}\sum_{\sigma\sigma'}\sum_{ll'}\frac{e^2}{|\mathbf{R}_N+\mathbf{r}_l-\mathbf{R}_{N'}-\mathbf{r}_{l'}|}l^{\dagger}_{N\sigma}l'^{\dagger}_{N'\sigma'}l'_{N'\sigma'}l_{N\sigma}, \tag{3}$$

and H^{ext} is the coupling Hamiltonian which couples the external fields to the intercell and intracell charge fluctuations:

$$H^{\mathrm{ext}}\approx\sum_{N\sigma l}\{eV^{\mathrm{ext}}_{l}(\mathbf{Q},\omega)e^{\mathbf{i}[\mathbf{Q}\cdot(\mathbf{R}_N+\mathbf{r}_l)-\omega t]+\eta t}l^{\dagger}_{N\sigma}l_{N\sigma}+\mathrm{H.c.}\}. \tag{4}$$

Vectors $\mathbf{r}_l$ are attributed to the positions of the copper and oxygen ions within the two-dimensional (2D) unit cell; thus the index $l\in\{d,p_x,p_y\}$. We shall draw here a distinction between the 3D vectors and the 2D vectors by using, respectively, the upper and lower case letters. For example, the Bravais lattice vector $\mathbf{R}_N=\Sigma_{i=1}^{3}n_i\mathbf{a}_i\equiv(\mathbf{R}_n,n_3)$ or the wave vector $\mathbf{K}\equiv(\mathbf{k},k_z)$. In this sense note that the expressions (2) and (4) contain only the intraplane contributions, while in the Hamiltonian (3) there are both the intraplane and interplane interactions. In $\mathcal{H}_0$ it is also assumed that the overlap integrals between the neighboring layers $t_{\perp}$ are negligible.

Let us briefly recall the structure of the 2D bare Hamiltonian for both the case where $U_d=0$ and the case in which the large U_d is present. The motivation for simultaneous treatment of these two cases is the fact that for $U_d\rightarrow\infty$, described by the mean-field approximation of the slave-boson approach, H has the same structure as for $U_d=0$. Consequently, both physical situations will be represented by the same formalism, and will be the subject of easy comparison.

It was previously shown that the large-U_d regime of the three-band model can be well described by the slave-boson approach.[15] The simplest formalism of this kind corresponds to the formal limit $U_d\rightarrow\infty$. For the latter, the 2D bare Hamiltonian takes the form

$$\mathcal{H}_0=H_0(\lambda,b)+N\lambda(b^2-1), \tag{5}$$

$$H_0(\lambda,b)=\sum_{n\sigma}[E_d d^{\dagger}_{n\sigma}d_{n\sigma}+E_p(p^{\dagger}_{xn\sigma}p_{xn\sigma}+p^{\dagger}_{yn\sigma}p_{yn\sigma})]$$
$$+\sum_{n\sigma}t_{pd}[(p^{\dagger}_{xn\sigma}+p^{\dagger}_{yn\sigma})d_{n\sigma}$$
$$-(p^{\dagger}_{xn-a\sigma}+p^{\dagger}_{yn-b\sigma})d_{n\sigma}+\mathrm{H.\,c.}]. \tag{6}$$

Here $E_d=E^0_d+\lambda$ and $E_p=E^0_p$ are, respectively, the renormalized energies of one copper d and two oxygen p orbitals in the 2D unit cell, and $t_{pd}=bt^0_{pd}$ is the renormalized overlap energy. In the mean-field approximation for slave bosons, λ and b are quantities which have to be determined self-consistently by minimization of the thermodynamic potential Ω (see Appendix B). These expressions describe the $U_d=0$ limit as well, provided that $\lambda=0$ and $b=1$.

$H_0(\lambda,b)$ is the part of Hamiltonian which can be straightforwardly diagonalized. Although the results of this diagonalization procedure are well known, we put some of the corresponding expressions in Appendix A, in order to define the transformation-matrix elements $U_{\mathbf{k}}(L,l)$ and the abbreviations for the factors frequently used in the text. It is important to remember that, for λ and b which were found relevant in the high-T_c superconductors (HTSC's) by the electric-field-gradient (EFG) analysis (see Fig. 1),[16,17] the matrix elements $U_{\mathbf{k}}(L,l)$ have to be used in the complete form. Evidently, a great simplification occurs in the narrow-band limit where the expansion of $U_{\mathbf{k}}(L,l)$ in terms of t_{pd}/Δ_{pd} is allowed.

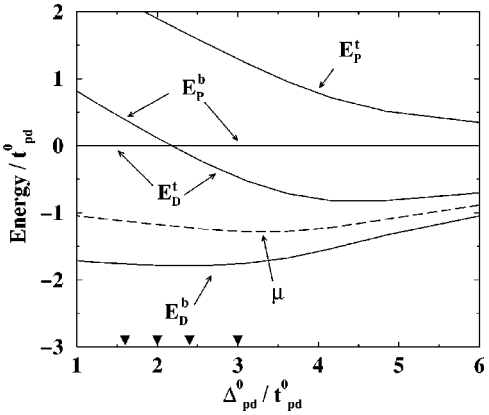

FIG. 1. Dependence of the tops and bottoms (E^t_L and E^b_L) of the bonding and antibonding bands, as well as the chemical potential μ, on the parameter $\Delta^0_{pd}=E^0_p-E^0_d$, for $U_d\rightarrow\infty$, $\delta=0.2$. Here $E_p=0$ is chosen. The values $\Delta^0_{pd}/t^0_{pd}=1.6$, 2.0, 2.4, and 3.0 estimated in the EFG analysis in $HgBa_2CuO_{4.11}$, $Tl_2Ba_2CuO_6$, $YBa_2Cu_3O_7$, and $La_{1.85}Sr_{0.15}CuO_4$ compounds are labeled by filled triangles (Refs. 16 and 17).

The 3D bare Hamiltonian will be given on replacing vectors $\mathbf{R}_n$ and $\mathbf{k}$ in Eqs. (5), (6), (A2), and (A3) with associated 3D vectors $\mathbf{R}_N$ and $\mathbf{K}$. Now

$$\mathcal{H}_0=\sum_{L\mathbf{K}\sigma}E_L(\mathbf{K})L^{\dagger}_{\mathbf{K}\sigma}L_{\mathbf{K}\sigma}+N\lambda(b^2-1), \tag{7}$$

with the band index $L\in\{D,P,N\}$. According to Eq. (2), the Bloch energies $E_L(\mathbf{K})$ and the matrix elements $U_{\mathbf{K}}(L,l)$ are independent of k_z. In a more realistic case, where $t_{\perp}$ are finite but $|t_{\perp}|\ll|t^0_{pd}|$, it still holds:[18]

$$E_L(\mathbf{K})\approx E_L(\mathbf{k})+\mathcal{O}(1/m^L_{zz}),$$
$$U_{\mathbf{K}}(L,l)\approx U_{\mathbf{k}}(L,l). \tag{8}$$

To keep a general form of the RPA equations done below, from here on we will assume the approximate relations (8) rather than the exact $t_{\perp}=0$ relations.

The simplest way to describe how the Raman-active phonons will affect the electronic properties is to treat the phonons as the external fields which will be coupled to the holes through the Hamiltonian (4). In the Bloch representation one obtains

$$H^{\mathrm{ext}}\approx\sum_{\mathbf{K}'\sigma' l}\sum_{L_1L_2}[U_{\mathbf{k}'}(l,L_1)U^{*}_{\mathbf{k}'-q}(l,L_2)$$
$$\times eV^{\mathrm{ext}}_{l}(\mathbf{Q},\omega)e^{-\mathrm{i}\,\omega t+\eta t}L^{\dagger}_{1\mathbf{K}'\sigma'}L_{2\mathbf{K}'-\mathbf{Q}\sigma'}+\mathrm{H.c.}]. \tag{9}$$

Here $\mathbf{Q}$'s are restricted to the first Brillouin zone (IBZ). The coefficients $V_l^{\rm ext}(\mathbf{Q},\omega)$ can be easily arranged according to the irreducible representations of the D_{4h} group, which characterize the Raman-active phonons of the HTSC's, giving only the coupling between the phonons and the intracell charge fluctuations of the same symmetry. As can be easily seen, this Hamiltonian shows also how an actual external potential [given by $V_l^{\rm ext}(\mathbf{Q},\omega)=V^{\rm ext}(\mathbf{Q},\omega)$] will be coupled to the intercell charge fluctuations.

In terms of the Bloch operators, the interacting Hamiltonian reads as

$$H^{\rm c}\approx\frac{1}{2}\sum_{\mathbf{K}'\mathbf{K}''\mathbf{Q}'}\frac{1}{V}\frac{4\pi e^2}{Q'^2}\sum_{\sigma'\sigma''}\sum_{ll'}\sum_{L_1L_2L_3L_4}\times U_{\mathbf{k}'}(l,L_1)U_{\mathbf{k}''}(l',L_2)U^*_{\mathbf{k}''+\mathbf{q}'}(l',L_3)\times U^*_{\mathbf{k}'-\mathbf{q}'}(l,L_4)L^\dagger_{1\mathbf{K}'\sigma'}L^\dagger_{2\mathbf{K}''\sigma''}L_{3\mathbf{K}''+\mathbf{Q}'\sigma''}L_{4\mathbf{K}'-\mathbf{Q}'\sigma'}, \tag{10}$$

i.e., only monopole-monopole interactions are present in the considered long-wavelength limit of the Emery model. Our purpose here is to resolve a few simple (but general) issues related to the optical conductivity and Raman spectra. In this respect note that, after omitting the short-range interactions among the intracell charge fluctuations, it is impossible for the pure electronic intracell collective modes to appear directly in the Raman response.

B. Random-phase approximation

The linear response of the electronic system can be formulated by using the observable $L^\dagger_{1\mathbf{K}\sigma}L_{2\mathbf{K}+\mathbf{Q}\sigma}$. To find the time dependence of its expectation value in the presence of the external fields, the Schödinger picture can be used, in which we have

$$\mathrm{i}\hbar\frac{\partial}{\partial t}\delta\langle\Psi|L^\dagger_{1\mathbf{K}\sigma}L_{2\mathbf{K}+\mathbf{Q}\sigma}|\Psi\rangle=\langle\Psi|[L^\dagger_{1\mathbf{K}\sigma}L_{2\mathbf{K}+\mathbf{Q}\sigma},H]|\Psi\rangle, \tag{11}$$

where $|\Psi\rangle$ is the perturbed ground-state wave function equal to the sum of the unperturbed one $|\Psi_0\rangle$ and the correction $|\delta\Psi\rangle$, which contains contributions of all orders in perturbation. Here

$$\delta\langle\Psi|L^\dagger_{1\mathbf{K}\sigma}L_{2\mathbf{K}+\mathbf{Q}\sigma}|\Psi\rangle\equiv\langle\Psi_0|L^\dagger_{1\mathbf{K}\sigma}L_{2\mathbf{K}+\mathbf{Q}\sigma}|\delta\Psi\rangle+\langle\delta\Psi|L^\dagger_{1\mathbf{K}\sigma}L_{2\mathbf{K}+\mathbf{Q}\sigma}|\Psi_0\rangle. \tag{12}$$

Using Eq. (12), it is possible to express the Fourier transform of the induced charge density on the l orbital as

$$\rho_l^{\rm ind}(\mathbf{Q},\omega)=\frac{e}{V}e^{\mathrm{i}\omega t}\sum_{\mathbf{K}\sigma}\sum_{L_1L_2}U_{\mathbf{k}}(l,L_1)U^*_{\mathbf{k}+\mathbf{q}}(l,L_2)\times\delta\langle\Psi|L^\dagger_{1\mathbf{K}\sigma}L_{2\mathbf{K}+\mathbf{Q}\sigma}|\Psi\rangle. \tag{13}$$

For the Hamiltonian (1), the induced densities are given by the RPA matrix equation which is of the form

$$\rho^{\rm ind}(\mathbf{Q},\omega)=\chi(\mathbf{Q},\omega)V^{\rm ext}(\mathbf{Q},\omega)+\chi(\mathbf{Q},\omega)V(\mathbf{Q})\rho^{\rm ind}(\mathbf{Q},\omega). \tag{14}$$

Here $\rho^{\rm ind}(\mathbf{Q},\omega)$, $V^{\rm ext}(\mathbf{Q},\omega)$, $V(\mathbf{Q})$, and $\chi(\mathbf{Q},\omega)$ are the matrices which elements are respectively $\rho_l^{\rm ind}(\mathbf{Q},\omega)$, $V_l^{\rm ext}(\mathbf{Q},\omega)$, $V_{ll'}(\mathbf{Q})=4\pi/Q^2$, and

$$\chi_{ll'}(\mathbf{Q},\omega)=\frac{1}{V}\sum_{\mathbf{K}\sigma}\sum_{L_1L_2}R_l^{L_1L_2}(\mathbf{k},\mathbf{k}+\mathbf{q})R_{l'}^{L_2L_1}(\mathbf{k}+\mathbf{q},\mathbf{k})\times\frac{f_{L_1}(\mathbf{K})-f_{L_2}(\mathbf{K}+\mathbf{Q})}{\hbar\omega-E_{L_2}(\mathbf{K}+\mathbf{Q})+E_{L_1}(\mathbf{K})+\mathrm{i}\,\eta}. \tag{15}$$

For convenience, the charge-vertex functions are introduced:

$$R_l^{L_1L_2}(\mathbf{k},\mathbf{k}')=eU_{\mathbf{k}}(l,L_1)U^*_{\mathbf{k}'}(l,L_2). \tag{16}$$

The Fermi-Dirac function $[1+e^{\beta[E_L(\mathbf{K})-\mu]}]^{-1}$ is denoted by $f_L(\mathbf{K})$.

As it is previously shown in the $\mathbf{q}=0$ analyses of the three-band model,[19] instead of the above matrix representation, another one is particularly useful (here called the $\nu\mathbf{K}$ representation) because it enables a natural separation between the intercell and intracell charge fluctuations. This representation is very convenient in the limit of long wavelengths. It is connected with the first one by two transformation matrices:

$$A^\dagger=\frac{1}{2}\begin{pmatrix}1 & 1 & 0\\ 1/2 & -1/2 & 1\\ 1/2 & -1/2 & -1\end{pmatrix},\qquad B=\begin{pmatrix}1 & 1 & 1\\ 1 & -1 & -1\\ 0 & 1 & -1\end{pmatrix},$$

$$A^\dagger B=B^\dagger A=1. \tag{17}$$

The following induced densities become relevant:

$$\rho_\nu^{\rm ind}(\mathbf{Q},\omega)=\sum_l B_{\nu l}\rho_l^{\rm ind}(\mathbf{Q},\omega), \tag{18}$$

with the intercell charge transfer, the intracell charge transfer of the pd symmetry (usual notation A_{1g}, see Appendix C), and the intracell charge transfer of the pp symmetry (B_{1g} or B_{2g}) corresponding to $\nu=1$, 2, and 3, respectively. The fields which couple directly to these densities are

$$V_\nu^{\rm ext}(\mathbf{Q},\omega)=\sum_l A_{\nu l}V_l^{\rm ext}(\mathbf{Q},\omega). \tag{19}$$

According to Eq. (10), the only nonvanishing term in the new Coulomb matrix is

$$V_{\nu\nu'}(\mathbf{Q})=\sum_{ll'}A_{\nu l}V_{ll'}(\mathbf{Q})A^\dagger_{l'\nu'}=\delta_{\nu,1}\delta_{\nu',1}V_{11}(\mathbf{Q}), \tag{20}$$

with $V_{11}(\mathbf{Q})=4\pi/Q^2$. In spite of this restriction on $V_{\nu\nu'}(\mathbf{Q})$, the interplay between the intercell and intracell charge fluc-

tuations will occur in Eq. (14) due to the off-diagonal terms in the susceptibility matrix.[20] The matrix takes the form

$$\chi_{\nu\nu'}(\mathbf{Q},\omega)=\sum_{ll'} B_{\nu l}\chi_{ll'}(\mathbf{Q},\omega)B^{\dagger}_{l'\nu'}$$
$$=\frac{1}{V}\sum_{\mathbf{K}\sigma}\sum_{L_1L_2} R_{\nu}^{L_1L_2}(\mathbf{k},\mathbf{k}+\mathbf{q})R_{\nu'}^{L_2L_1}(\mathbf{k}+\mathbf{q},\mathbf{k})$$
$$\times\frac{f_{L_1}(\mathbf{K})-f_{L_2}(\mathbf{K}+\mathbf{Q})}{\hbar\omega-E_{L_2}(\mathbf{K}+\mathbf{Q})+E_{L_1}(\mathbf{K})+\mathrm{i}\,\eta}, \qquad (21)$$

where the charge-vertex functions are rearranged into one monopole ($\nu=1$) and two quadrupole ($\nu=2$ and 3) terms, which are given by

$$R_{\nu}^{LL'}(\mathbf{k},\mathbf{k}')=\sum_{l} B_{\nu l}R_{l}^{LL'}(\mathbf{k},\mathbf{k}'). \qquad (22)$$

The RPA equations which we consider here are thus of the form

$$\rho_{\nu_1}^{\mathrm{ind}}(\mathbf{Q},\omega)=\chi_{\nu_1\nu}(\mathbf{Q},\omega)V_{\nu}^{\mathrm{ext}}(\mathbf{Q},\omega)$$
$$+\chi_{\nu_1 1}(\mathbf{Q},\omega)V_{11}(\mathbf{Q})\rho_1^{\mathrm{ind}}(\mathbf{Q},\omega). \qquad (23)$$

C. Dielectric function

In the longitudinal approach, the dielectric function follows from the Dyson equation for the screened monopole-monopole interaction rewritten in the form

$$\tilde{V}_{11}(\mathbf{Q},\omega)=\frac{V_{11}(\mathbf{Q})}{\varepsilon(\mathbf{Q},\omega)}. \qquad (24)$$

From Eqs. (7), (10), and (20), it straightforwardly follows that

$$\tilde{V}_{11}(\mathbf{Q},\omega)=V_{11}(\mathbf{Q})+V_{11}(\mathbf{Q})\chi_{11}(\mathbf{Q},\omega)\tilde{V}_{11}(\mathbf{Q},\omega), \qquad (25)$$

and

$$\varepsilon(\mathbf{Q},\omega)=1-\frac{4\pi}{Q^2}\chi_{11}(\mathbf{Q},\omega). \qquad (26)$$

Note that in the present long-wavelength formalism there is the interband term $\chi_{11}^{\mathrm{inter}}(\mathbf{Q},\omega)$ in the dielectric function [$L_1L_2=DP$, PD, DN, and ND in Eq. (21)], in addition to the usual intraband one $\chi_{11}^{\mathrm{intra}}(\mathbf{Q},\omega)$ ($L_1L_2=DD$). Since all associated charge vertices $R_{\nu}^{L_1L_2}(\mathbf{k}+\mathbf{q},\mathbf{k})$ are proportional to $\mathbf{q}$, the term $\chi_{11}^{\mathrm{inter}}(\mathbf{Q},\omega)$ was hidden in the $\mathbf{q}=0$ considerations.[21,13]

Not surprisingly, the transformation of the RPA Eqs. (23) into the diagonal form

$$\rho_{\nu}^{\mathrm{ind}}(\mathbf{Q},\omega)=\tilde{\chi}_{\nu\nu}(\mathbf{Q},\omega)V_{\nu}^{\mathrm{ext}}(\mathbf{Q},\omega) \qquad (27)$$

leads to the same structure of $\varepsilon(\mathbf{Q},\omega)$. Here $\tilde{\chi}_{\nu\nu}(\mathbf{Q},\omega)$ are the screened charge-charge correlation functions. Let us now consider the elements of the unscreened and screened susceptibility matrices $\chi(\mathbf{Q},\omega)$ and $\tilde{\chi}(\mathbf{Q},\omega)$ in some detail. In the next paragraph we turn to a more detailed discussion of these functions.

The symmetry of $R_{\nu}^{LL'}(\mathbf{k},\mathbf{k}')$ determines the symmetry of $\chi_{\nu\nu'}(\mathbf{Q},\omega)$ and influences the way in which these elements of the susceptibility matrix will be screened in the RPA. The leading term in Taylor series expansion

$$R_{\nu}^{LL'}(\mathbf{k}+\mathbf{q},\mathbf{k})\approx R_{\nu}^{LL'}(\mathbf{k},\mathbf{k})+\mathbf{q}\cdot\nabla_{\mathbf{k}'}R_{\nu}^{LL'}(\mathbf{k}',\mathbf{k})|_{\mathbf{k}'=\mathbf{k}}+\cdots \qquad (28)$$

is entirely sufficient for the long wavelengths. For the nearly half filled bonding band only those charge vertices $R_{\nu}^{LL'}(\mathbf{k},\mathbf{k}')$ are interesting in which L or L' are equal to D. The explicit form of leading contributions to all these vertices in the limit of long wavelengths are given in Appendix C. Here we only notice the following: (i) The intercell charge transfer in the interband channel is characterized by $R_1^{LL'}(\mathbf{k}+\mathbf{q},\mathbf{k})\propto q$, as mentioned above. (ii) All $R_3^{LL'}(\mathbf{k},\mathbf{k}')$ elements are antisymmetric at least for one among the symmetry operations $x\rightleftharpoons y$, $x\rightarrow -x$, or $y\rightarrow -y$. The consequence of first observation is that, although it is proportional to q^2, the interband correlation function $\chi_{11}^{\mathrm{inter}}(\mathbf{Q},\omega)$ becomes important in the RPA, because it is multiplied by $4\pi/Q^2$, and therefore will be important in the explanation of the high-frequency properties of the three-band model. Similarly, the pp charge fluctuations will not be coupled with other two fluctuations because of the symmetry (ii). Therefore the unscreened susceptibility matrix can be decomposed into two submatrices:

$$\chi(\mathbf{Q},\omega)=\begin{pmatrix}\chi_{11}(\mathbf{Q},\omega) & \chi_{12}(\mathbf{Q},\omega) & 0\\ \chi_{21}(\mathbf{Q},\omega) & \chi_{22}(\mathbf{Q},\omega) & 0\\ 0 & 0 & \chi_{33}(\mathbf{Q},\omega)\end{pmatrix}. \qquad (29)$$

On the other hand, the screened susceptibility matrix $\tilde{\chi}(\mathbf{Q},\omega)$ is diagonal by definition (27). The corresponding elements are

$$\tilde{\chi}_{11}(\mathbf{Q},\omega)=\frac{\chi_{11}(\mathbf{Q},\omega)}{\varepsilon(\mathbf{Q},\omega)},$$
$$\tilde{\chi}_{22}(\mathbf{Q},\omega)=\chi_{22}(\mathbf{Q},\omega)+\chi_{21}(\mathbf{Q},\omega)\frac{V_{11}(\mathbf{Q})}{\varepsilon(\mathbf{Q},\omega)}\chi_{12}(\mathbf{Q},\omega),$$
$$\tilde{\chi}_{33}(\mathbf{Q},\omega)=\chi_{33}(\mathbf{Q},\omega). \qquad (30)$$

It is important to note that both the intraband and interband contributions in all these functions are entirely described by parameters of the starting bare Hamiltonian, as in a recently given analysis of the dielectric properties of the dipolar crystals.[22] There is no need for phenomenological parameters commonly used in the description of the interband terms.[23,24] But, unlike in the dipolar crystals, the Lorentz-Lorenz form of the interband contribution to the dielectric function does not appear in the present three-band model.

Evidently, for one interested in the Raman-active phonons, the functions $\tilde{\chi}_{22}(\mathbf{Q},\omega_0)$ and $\tilde{\chi}_{33}(\mathbf{Q},\omega_0)$ are important, where ω_0 is the phonon frequency. The result (30)

clearly explains that both functions $\tilde{\chi}_{22}^{\text{intra}}(\mathbf{Q},\omega_0)$ and $\tilde{\chi}_{33}^{\text{intra}}(\mathbf{Q},\omega_0)$ remain finite, and that the measured phonon self-energies (their anomalies in particular) are presumably related with the intraband processes.

Susceptibility matrix

Let us first see the limit of the *weak splitting* $\Delta_{pd}\equiv E_p - E_d \ll t_{pd}$, which is characterized by the pd ''dimerization'' gap. The magnitude of the gap is proportional to Δ_{pd}, and its wave vector is equal to $\pm(2\pi/a,2\pi/a,0)$. It is convenient to reduce this problem additionally by omitting both the interband contributions related to the nonbonding band and the pp charge fluctuations. The susceptibility matrix takes now the form

$$\chi(\mathbf{Q},\omega)=\begin{pmatrix}\chi_{11}(\mathbf{Q},\omega) & \chi_{12}(\mathbf{Q},\omega)\\ \chi_{21}(\mathbf{Q},\omega) & \chi_{22}(\mathbf{Q},\omega)\end{pmatrix}, \tag{31}$$

which is common for all models with site-energy dimerization. Although the difference $u_{\mathbf{k}}^2-v_{\mathbf{k}}^2$ is a complicated function of Δ_{pd}, the factor Δ_{pd} can be easily recognized in it, due to the relation

$$t_{\mathbf{k}}(u_{\mathbf{k}}^2-v_{\mathbf{k}}^2)=-\Delta_{pd}u_{\mathbf{k}}v_{\mathbf{k}}. \tag{32}$$

Thus it will vanish in the limit $\Delta_{pd}\to 0$. Two charge vertices $R_1^{DP}(\mathbf{k}+\mathbf{q},\mathbf{k})$ and $R_2^{DD}(\mathbf{k}+\mathbf{q},\mathbf{k})$, which are proportional to this difference, disappear for $\mathbf{q}\to 0$, $\Delta_{pd}\to 0$ as well, so that the expression (31) reduces to

$$\chi(\mathbf{Q},\omega)=\begin{pmatrix}\chi_{11}^{\text{intra}}(\mathbf{Q},\omega) & 0\\ 0 & \chi_{22}^{\text{inter}}(\mathbf{Q},\omega)\end{pmatrix}. \tag{33}$$

After eliminating the nonbonding band, closing the dimerization gap makes the bonding and antibonding bands appear as two parts of a single square-lattice band with twice the original Brillouin zone. It turns out also that $\rho_2^{\text{ind}}(\mathbf{Q},\omega)\equiv\rho_1^{\text{ind}}[\mathbf{Q}\pm(2\pi/a,2\pi/a,0),\omega]$, and only one kind of the charge fluctuations $[\rho_1^{\text{ind}}(\mathbf{Q},\omega)]$ exists in this case.

In the three-band model the above decoupling occurs in the $\Delta_{pd}\to 0$ limit indeed. But, in contrast to the simple models with the site-energy dimerization, here the lattice does not undergo the unit-cell transformation, since the symmetry of the lattice is not changed for $\Delta_{pd}=0$ and thus the original symmetry of the whole crystal is retained. The above weak splitting consideration explains the fact that the vertices $R_1^{DP}(\mathbf{k}+\mathbf{q},\mathbf{k})$ and $R_2^{DD}(\mathbf{k}+\mathbf{q},\mathbf{k})$ describe those interband and intraband processes of the electronic system in which the dimerization potential dissipates an extra momentum $\pm\hbar(2\pi/a,2\pi/a,0)$.

This issue can be reconsidered in a more general frame as well, with a dimerization gap $\Delta_{pp}\equiv E_{p_x}-E_{p_y}$ also present. Several new terms in $\chi_{\nu\nu'}(\mathbf{Q},\omega)$ appear in this case. Since the symmetry $x\rightleftharpoons y$ is broken, some off-diagonal terms $\chi_{\nu\nu'}(\mathbf{Q},\omega)$, $\nu=3$ or $\nu'=3$ become finite, leading possibly to the coupling between the intercell and pp intracell charge fluctuations, and to a more complicated form of the screened pp charge correlation function $\tilde{\chi}_{33}(\mathbf{Q},\omega)$.

To conclude, whenever the regime $\Delta_{pp}=0$ is in question, the results (30) can be used. Especially valuable consequence of Eqs. (30) is that the pp charge correlation function does not suffer screening, even in the static, long-wavelength limit, in contrast to the intercell charge correlation function which will be totally screened out and the intraband part of the pd charge correlation function which will be mostly screened in this limit. It is previously shown that, even when the short-range forces are taken into account, the off-diagonal terms $V_{\nu\nu'}(\mathbf{Q})$, $\nu=3$ or $\nu'=3$, remain zero.[11] Therefore the function $\tilde{\chi}_{33}(\mathbf{Q},\omega)$ will be screened in Eq. (14) neither via the off-diagonal terms of the susceptibility matrix nor of the Coulomb matrix.

Although in the static limit the intraband part of the pd charge correlation function does not disappear in general, it can be shown from

$$\tilde{\chi}_{22}^{\text{intra}}(\mathbf{Q}\approx 0,0)=\chi_{22}^{\text{intra}}(\mathbf{Q}\approx 0,0)+\frac{4\pi}{Q^2\varepsilon(\mathbf{Q}\approx 0,0)}\times\chi_{21}^{\text{intra}}(\mathbf{Q}\approx 0,0)\chi_{12}^{\text{intra}}(\mathbf{Q}\approx 0,0) \tag{34}$$

that in two particular cases it will. First, in the weak-splitting limit $\Delta_{pd}\to 0$ the vertex $R_2^{DD}(\mathbf{k}+\mathbf{q},\mathbf{k})$ and thus the function $\tilde{\chi}_{22}^{\text{intra}}(\mathbf{Q}\approx 0,0)$ are negligible. Similarly, for the *strong-splitting* limit $\Delta_{pd}\gg t_{pd}$ follows $R_2^{DD}(\mathbf{k}+\mathbf{q},\mathbf{k})\approx R_1^{DD}(\mathbf{k}+\mathbf{q},\mathbf{k})$ and $\tilde{\chi}_{22}^{\text{intra}}(\mathbf{Q}\approx 0,0)\approx\tilde{\chi}_{11}^{\text{intra}}(\mathbf{Q}\approx 0,0)\propto Q^2$. This means that in the strong-splitting limit, with the static screening included, the susceptibility (31) takes the form which is known from the previous $\mathbf{q}=0$ analysis of the three-band model[21]

$$\tilde{\chi}(0,0)=\begin{pmatrix}0 & 0\\ 0 & \chi_{22}^{\text{inter}}(0,0)\end{pmatrix}. \tag{35}$$

III. COMPARISON WITH EXPERIMENTS

There are numerous measurements on the HTSC's the results of which are closely related to the questions discussed in the last section. We shall put now some of these questions in the experimental context. We shall first discuss the Raman-active optical phonons in the $YBa_2Cu_3O_{7-x}$ materials[4,5] and then examine some details of the optical-conductivity spectra.[1–3]

A. Raman-active phonons

The Raman-active optical phonons represent a powerful probe of the electronic system at optical frequencies.[4,5] In the materials with two molecules CuO_2 per primitive cell ($M\,Ba_2Cu_3O_{7-x}$, $M=$Y, Eu, Gd, for example) several Raman-active phonons are found. To treat the effect of the electronic system on one of these phonons (characterized by ν and $\mathbf{Q}$, in the tetragonal lattices), we start with the Hamiltonian

$$H=\mathcal{H}_0+H^{\text{c}}+H^{\text{el-ph}}+H^{\text{ph}}. \tag{36}$$

TABLE I. The electron-phonon coupling constants α_l and α_ν for five Raman-active phonons of $YBa_2Cu_3O_7$. According to the EFG analysis (Ref. 16), the average ion charges 3, 2, 1.54, 1.64, −1.71, −1.72, −1.72, and −1.52 for, respectively, Y, Ba, Cu(1), Cu(2), O(1), O(2), O(3), and O(4) ions are used in the calculation. The frequencies are from Ref. 5.

		$\omega[\mathrm{cm}^{-1}]$	α_d	α_{p_x}	α_{p_y}	α_2	α_3
A_{1g}	Ba↑	132	1.94	2.23	2.25	0.15	−0.01
	Cu(2)↑	150	1.59	1.72	1.70	0.15	−0.01
	O(2)↑ O(3)↑	440	−1.39	−2.01	−2.03	0.32	0.01
	O(1)↑	500	−2.04	−1.69	−1.68	−0.18	−0.01
B_{1g}	O(2)↑ O(3)↓	340	0.00	0.49	−0.56	0.02	0.52

Here $H^{\mathrm{el-ph}}$ is the coupling Hamiltonian (9) shown in the $\nu\mathbf{K}$ representation, with the fields $V_\nu^{\mathrm{ext}}(\mathbf{Q},\omega)$ expressed in terms of the phonon operators $a^\dagger_{\nu\mathbf{Q}}$, and H^{ph} is the phonon Hamiltonian

$$H^{\mathrm{ph}}=\hbar\omega_0 a^\dagger_{\nu\mathbf{Q}}a_{\nu\mathbf{Q}}. \tag{37}$$

There are a few questions which have to be addressed here. First of all, the orthorhombic distortion of the lattices mixes up the symmetries A_{1g} and B_{1g}, so that in the superconducting compounds $YBa_2Cu_3O_{7-x}$ (where the data given in Table I are taken) all the considered phonons and the relevant intracell charge fluctuations belong to the representation A_g. Consequently, to employ reasonably the results of preceding section in these compounds, the rate of this admixture has to be estimated. As argued below, for the phonons this admixture is of order 1/15. Second, the electron-phonon coupling will be also affected by the electronic interband excitations. But, until the characteristic energies of the excitations are significantly larger than the phonon energy, these corrections are expected to be negligible and only the intraband processes are relevant [which are of the A_{1g} or B_{1g} symmetry, according to Eq. (C1)]. Third, to describe correctly the screened electron-phonon coupling constants in the A_{1g} channel, it is necessary to throw away the static screening, as discussed above.

Finally, we find

$$H^{\mathrm{el-ph}}\approx\frac{1}{\sqrt{N}}\sum_{\mathbf{K}\sigma}G_\nu(\mathbf{K}+\mathbf{Q},\mathbf{K})R_\nu^{DD}(\mathbf{k}+\mathbf{q},\mathbf{k})\times D^\dagger_{\mathbf{K}+\mathbf{Q}\sigma}D_{\mathbf{K}\sigma}(a_{\nu\mathbf{Q}}+a^\dagger_{\nu-\mathbf{Q}}). \tag{38}$$

As it was previously shown,[8] the leading contribution to the electron-phonon coupling constant $G_\nu(\mathbf{K}+\mathbf{Q},\mathbf{K})$ for the Raman-active phonons does not depend on the wave vectors. In the ionic model of the electron-phonon coupling the result

$$G_\nu(\mathbf{K}+\mathbf{Q},\mathbf{K})=\sqrt{\frac{\hbar}{2M_{l_0}\omega_0}}e_z(l_0,\nu)\frac{e\alpha_\nu}{|\mathbf{r}_d-\mathbf{r}_{p_x}|^2} \tag{39}$$

is obtained. Here M_{l_0} is the mass of one among the ions involved and $e_z(l_0,\nu)$ is the corresponding normalization constant [structure of the constant $e_z(l_0,\nu)$ for a few examples can be found in Ref. 12]. The dimensionless constants α_2 and α_3 can be easily found for each phonon mode of interest, by using $\alpha_\nu=\Sigma_l A_{\nu l}\alpha_l$. The values of α_l and α_ν for five Raman-active phonons are given in Table I, obtained with the aid of the Ewald method and the point-charge approximation. In the calculation the average ionic charges q_i estimated in the EFG analysis are used.[16] (The procedure of calculation α_l can be found in Ref. 8. The accuracy of this calculation can be illustrated by comparing the calculated value $e\alpha_{p_x}/|\mathbf{r}_d-\mathbf{r}_{p_x}|^2\approx 2$ V/Å with the corresponding experimentally estimated values 1.3 V/Å and 1.53 V/Å reported in Ref. 25.) As shown in Table I, it is confirmed that the Raman-active phonon at 340 cm^{-1} is of the pp symmetry (i.e., B_{1g}) and all the other of the pd symmetry (A_{1g}), with 1 in 15 accuracy. At this level of approximation, the coupling Hamiltonian (38) can be used in the orthorhombic $YBa_2Cu_3O_{7-x}$ compounds, as well.

The influence of the interacting electrons on the phonon properties can be summarized by showing the phonon self-energies

$$\Sigma_\nu(\mathbf{Q},\omega_0)\approx|G_\nu|^2\tilde{\chi}^{\mathrm{intra}}_{\nu\nu}(\mathbf{Q},\omega_0), \tag{40}$$

where the arguments of the electron-phonon coupling constants are suppressed, the interband terms $\tilde{\chi}^{\mathrm{inter}}_{\nu\nu}(\mathbf{Q},\omega_0)$ as well (see the corresponding diagrams shown in Fig. 2). Similarly, the screened electron-phonon vertices can be written in the form

$$\tilde{G}_2R_2^{DD}(\mathbf{k}+\mathbf{q},\mathbf{k})=G_2\left[R_2^{DD}(\mathbf{k}+\mathbf{q},\mathbf{k})+\chi^{\mathrm{intra}}_{21}(\mathbf{Q},\omega_0)\frac{V_{11}(\mathbf{Q})}{\varepsilon(\mathbf{Q},\omega_0)}R_1^{DD}(\mathbf{k}+\mathbf{q},\mathbf{k})\right],$$

$$\tilde{G}_3R_3^{DD}(\mathbf{k}+\mathbf{q},\mathbf{k})=G_3R_3^{DD}(\mathbf{k}+\mathbf{q},\mathbf{k}). \tag{41}$$

Note that for the case of strong splitting $\tilde{G}_2R_2^{DD}(\mathbf{k}+\mathbf{q},\mathbf{k})\approx G_2R_2^{DD}(\mathbf{k}+\mathbf{q},\mathbf{k})/\varepsilon(\mathbf{Q},\omega_0)$ holds, with the further simplification $\tilde{G}_2=0$ and $\Sigma_2(\mathbf{Q},0)=0$ in the static limit. Clearly,

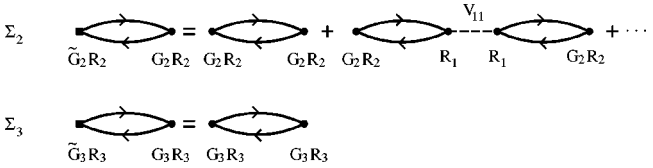

FIG. 2. The phonon self-energies $\Sigma_\nu(\mathbf{Q},\omega_0)$ and the screened electron-phonon coupling constants $\tilde{G}_\nu R_\nu^{DD}(\mathbf{k}+\mathbf{q},\mathbf{k})$ of the Raman-active phonons in the tetragonal lattices.

if the assumption of static screening were true, the electron-phonon coupling for the A_{1g} phonons would be exclusively given by the interband channels [which are neglected in Eqs. (40) and (41)]. This in particular means that all the A_{1g} phonons would exhibit a normal behavior, the hardening of the frequencies when the temperature decreases, regardless of the superconducting ordering. The experiments however deny this simplified scenario. Specifically, the measurements in $YBa_2Cu_3O_{7-x}$ had shown that the B_{1g} phonon exhibits in the superconducting phase the anomalous softening of the frequency with the decreasing of temperature,[4] in contrast to all other phonons for which this effect is significantly smaller, but does not vanish.

In conclusion, the expressions (40) and (41) incorporate most of the arguments mentioned in the previous discussions of this topic,[10,8,12] but, as mentioned above, underline a further one, that in order to describe the effect of the superconducting ordering on the phonon self-energies and to estimate the screened electron-phonon vertices, the dynamic screening (at $\omega=\omega_0$) has to be taken into account. This will lead to a finite change $\Sigma_2^s(\mathbf{Q},\omega_0)-\Sigma_2^n(\mathbf{Q},\omega_0)\propto\tilde{\chi}_{22}^{\text{intra},s}(\mathbf{Q},\omega_0)-\tilde{\chi}_{22}^{\text{intra},n}(\mathbf{Q},\omega_0)$ in particular, in accordance with the experiments, and in contrast to the previous conclusions based on the static-screening model.[10] (Here the indices n and s stand for the normal and the superconducting phase, respectively.)

Generally speaking, the scattering of electrons on impurities as well as the compatibility of the charge vertices $R_\nu^{DD}(\mathbf{k}+\mathbf{q},\mathbf{k})$ and the superconducting order parameter may also have a large impact on $\tilde{\chi}_{\nu\nu}^{\text{intra,s}}(\mathbf{Q},\omega_0)$.[10,6] If these dependences were brought into $\Sigma_\nu^s(\mathbf{Q},\omega_0)$ a complicated expression would be obtained, which cannot be fitted to the experimental data in any meaningful way.

B. Optical-conductivity measurements

To compare quantitatively the expression (26) with the optical data, it is necessary first to incorporate the relaxation processes in the analysis, at least in a phenomenological way. Two damping terms will be used here for this purpose, $\Sigma_1=\hbar/\tau$ for the intraband processes (τ is the usual relaxation time which includes the scattering of electrons on impurities and phonons) and Σ_2 for the interband ones (which describes, for example, the phonon-assisted interband processes).[23] Moreover, it is necessary to include in $\varepsilon(\mathbf{Q},\omega)$ the contributions of all other interband transitions for the bands which are not involved in the considered three-band model [see the term $\varepsilon_\infty(\mathbf{Q},\omega)$ in Eq. (42)]. Finally, it is essential to resolve the origin and structure of the anomalous mid-infrared contributions to the optical conductivity.

Our analysis of the optical data is evidently superficial in sense that the mid-infrared contributions are not taken into consideration. But, all other contributions are treated satisfactorily and might be used as a basis for further analyses of the optical data. At this level of approximation the relevant form of the microscopic dielectric function is

$$\varepsilon(\mathbf{Q},\omega)=\varepsilon_\infty(\mathbf{Q},\omega)-\frac{4\pi}{Q^2}[\chi_{11}^{\text{intra}}(\mathbf{Q},\omega,\Sigma_1)+\chi_{11}^{\text{inter}}(\mathbf{Q},\omega,\Sigma_2)]. \tag{42}$$

The corresponding macroscopic dielectric function can be obtained by using the dynamic, long-wavelength limit of Eq. (42). In the intraband term of $\chi_{11}(\mathbf{Q},\omega)$ it is convenient to use the following long-wavelength expansion of the Bloch energies:

$$E_D(\mathbf{K}+\mathbf{Q})\approx E_D(\mathbf{k})-\hbar\sum_{\alpha=x,y}v_\alpha(\mathbf{k})q_\alpha-\frac{\hbar^2}{2m}\sum_{\alpha=x,y}\sum_{\beta=x,y}\gamma_{\alpha\beta}(\mathbf{k})q_\alpha q_\beta+\cdots+\mathcal{O}(1/m_{zz}^D). \tag{43}$$

Here $v_\alpha(\mathbf{k})$ is the group velocity of electrons and $\gamma_{\alpha\beta}(\mathbf{k})$ is the static Raman-vertex function.[26] Similarly, in the corresponding interband term the expansions of the charge vertices (C2) and (C3) are useful.

Let us first briefly consider the anisotropy of the plasmon dispersion for the case $\mathbf{Q}=(q_x,q_y,q_z)$. Then follows the detailed comparison of the macroscopic dielectric function with the experimental data [the case where $\mathbf{Q}=(q_x,0,0)$ or $\mathbf{Q}=(0,q_y,0)$ will be assumed].

The dispersion of 3D plasmons $\omega_{pl}(\mathbf{Q})$ can be easily found by considering the real part of $\varepsilon(\mathbf{Q},\omega)$. When the plasmon energies $\hbar\omega_{pl}(\mathbf{Q})$ are smaller than the bare interband absorption edge $E_p-\mu$, the susceptibility $\chi_{11}^{\text{inter}}(\mathbf{Q},\omega,\Sigma_2)$ can be omitted in the equation

$$\text{Re}\{\epsilon(\mathbf{Q},\omega_{pl})\}=0 \tag{44}$$

in the first step. Furthermore, in this energy range it is expected that $\text{Re}\{\varepsilon_\infty(\mathbf{Q},\omega)\}\approx\varepsilon_\infty$. By using the limit $\Sigma_1\to 0$, one obtains a highly anisotropic dispersion

$$\omega_{pl}^2(\mathbf{Q})\approx\frac{4\pi e^2 n_e}{\varepsilon_\infty m_{xx}}\frac{q_x^2+q_y^2}{Q^2}\approx\Omega_{pl}^2\frac{Q_\parallel^2}{Q_\parallel^2+Q_\perp^2}, \tag{45}$$

exactly as expected for the 2D conductors. Here $(m_{xx})^{-1}=2a^2t_{pd}^2/(\hbar^2\Delta_{pd})$ is the mass scale which in the strong-splitting limit coincides with the diagonal components of the 2D reciprocal-electron-mass tensor. $\Omega_{pl}=\sqrt{4\pi e^2 n_e/(m_{xx}\varepsilon_\infty)}$ is the frequency of classical plasma, and $\mathbf{Q}_\parallel=(q_x,q_y,0)$, $\mathbf{Q}_\perp=(0,0,q_z)$. The effective concentration of conducting electrons n_e is defined here by

$$n_e=\frac{m_{xx}}{m}\frac{1}{V}\sum_{\mathbf{K}\sigma}(-)\gamma_{xx}(\mathbf{k})f_D(\mathbf{K}). \tag{46}$$

For the index $\alpha\in\{x,y\}$, the macroscopic dielectric function reads as

$$\varepsilon(q_\alpha,\omega)=\varepsilon_\infty(q_\alpha,\omega)-\frac{m}{m_{xx}}V_{pc}n_e\frac{(\hbar\Omega_0)^2}{\hbar\omega}\frac{\hbar\omega-i\Sigma_1}{(\hbar\omega)^2+\Sigma_1^2}$$
$$-\sum_{L=N,P}\frac{4\pi}{V}\sum_{\mathbf{K}\sigma}\left|\frac{\partial}{\partial k_\alpha}R_1^{LD}(\mathbf{k}',\mathbf{k})\right|^2_{\mathbf{k}'=\mathbf{k}}f_D(\mathbf{k})$$
$$\times\left(\frac{1}{\hbar\omega-E_L(\mathbf{k})+E_D(\mathbf{k})+i\Sigma_2}\right.$$
$$\left.-\frac{1}{\hbar\omega-E_D(\mathbf{k})+E_L(\mathbf{k})+i\Sigma_2}\right). \quad (47)$$

At the level of approximation used in Eq. (45), the real part of $\varepsilon(q_\alpha,\omega)$ takes the usual Drude-like form

$$\mathrm{Re}\{\varepsilon(q_\alpha,\omega)\}\approx\varepsilon_\infty-\frac{m}{m_{xx}}V_{pc}n_e\frac{(\hbar\Omega_0)^2}{(\hbar\omega)^2+\Sigma_1^2}. \quad (48)$$

The frequency of the in-plane plasma motion can be thus expressed in terms of three adjustable parameters ε_∞, m_{xx}/m, and τ (or Σ_1):

$$\Omega_{pl}^2=\frac{m}{m_{xx}}V_{pc}n_e\frac{\Omega_0^2}{\varepsilon_\infty}-1/\tau^2. \quad (49)$$

Note that the frequency $\Omega_0=\sqrt{4\pi e^2/(mV_{pc})}$, which is introduced here as the frequency-scale parameter, has in the $La_{2-x}Sr_xCuO_4$ compounds the value $\hbar\Omega_0\approx 3.8$ eV [$V_{pc}=a^2c/2$].

The imaginary part of $\varepsilon(q_\alpha,\omega)$ determines the real part of the optical conductivity $\sigma_{\alpha\alpha}(\omega)$. Since in the hole picture the absorption is characterized by $\omega<0$, one obtains

$$\mathrm{Re}\{\sigma_{\alpha\alpha}(\omega)\}=\frac{\omega}{4\pi}\mathrm{Im}\{\varepsilon(q_\alpha,\omega)\}$$
$$=\frac{m}{m_{xx}}V_{pc}n_e\frac{\Sigma_1}{(\hbar\omega)^2+\Sigma_1^2}\hbar\frac{\Omega_0^2}{4\pi}$$
$$+\sum_{L=N,P}\frac{1}{V}\sum_{\mathbf{K}\sigma}\left|\frac{\partial}{\partial k_\alpha}R_1^{LD}(\mathbf{k}',\mathbf{k})\right|^2_{\mathbf{k}'=\mathbf{k}}$$
$$\times\frac{-\omega\Sigma_2 f_D(\mathbf{k})}{[\hbar\omega-E_D(\mathbf{k})+E_L(\mathbf{k})]^2+\Sigma_2^2}$$
$$+\frac{\omega}{4\pi}\mathrm{Im}\{\varepsilon_\infty(q_\alpha,\omega)\}(\omega<0). \quad (50)$$

The first term in Eq. (50) is the Drude term. The second one describes the contribution of the interband transitions from the bonding band into the nonbonding and antibonding bands. Finally, the third one describes all other interband transitions. According to the presumptions of the three-band model, for $\Sigma_2\to 0$, the interband transitions start at the bare interband absorption edge $E_p-\mu$. In general, $\mathrm{Re}\{\sigma_{\alpha\alpha}(\omega)\}$ will depend on the fourth adjustable parameter Σ_2 as well, and, at higher energies in particular, on the structure of $\mathrm{Im}\{\varepsilon_\infty(q_\alpha,\omega)\}$.

The expressions (48)–(50) will be now compared with the optical data measured in the $La_{2-x}Sr_xCuO_4$ and $YBa_2Cu_3O_{6+x}$ compounds. The results are shown in Figs. 3–6. Note that, instead of the parameters t_{pd} and Δ_{pd} used in the previous sections, here we show the results in terms of the mass ratio m_{xx}/m and the bare interband absorption edge $E_p-\mu$. Good agreement is achieved for $m_{xx}/m=1.4$, $E_p-\mu=1.75$ eV, and $\varepsilon_\infty=4$ in $La_{1.8}Sr_{0.2}CuO_4$ and for $m_{xx}/m=0.4$, $E_p-\mu=1.5$ eV, and $\varepsilon_\infty=3$ in $YBa_2Cu_3O_{6.9}$. The conclusions of this comparison are as follows.

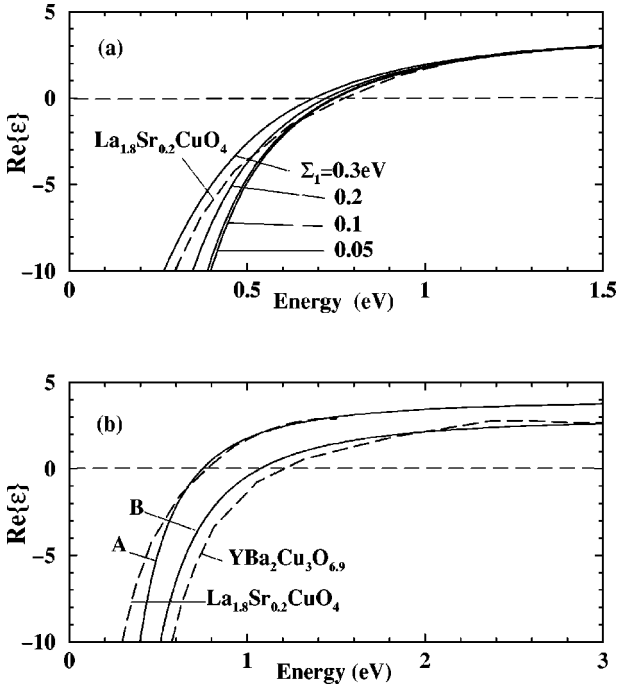

FIG. 3. The real part of the dielectric function as a function of relaxation time $\tau=\Sigma_1/\hbar$ (a) and mass ratio m_{xx}/m (b). The parameters which satisfactorily fit the measured data (long-dashed curves, from Refs. 2 and 3) are: $m_{xx}\approx 1.4m$, $\varepsilon_\infty=4$ [(a)]; $m_{xx}\approx 1.4m$, $\varepsilon_\infty=4$, $\Sigma_1=0.05$ eV [curve A in (b)]; $m_{xx}\approx 0.4m$, $\varepsilon_\infty=3$, $\Sigma_1=0.05$ eV [curve B in (b)].

The typical experimental value of the (in-plane) plasma energy in the superconducting $La_{2-x}Sr_xCuO_4$ compounds is $\hbar\Omega_{pl}\approx 0.8$ eV (see Fig. 3), in a significant departure from the standard free-electron value [corresponds to $m_{xx}/m=1$,

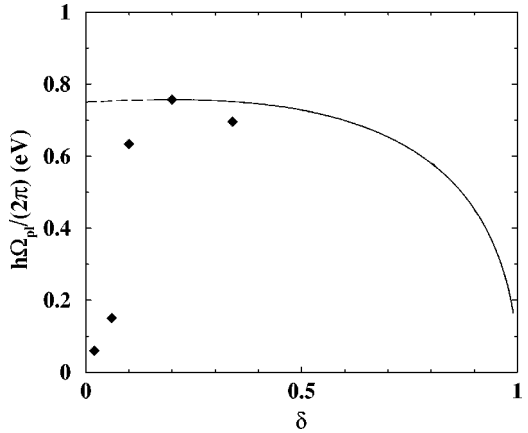

FIG. 4. Plasma frequency as a function of the doping δ in the case $U_d=0$ ($m_{xx}\approx 1.4m, \varepsilon_\infty=4, \Sigma_1=0.05$ eV). The experimental points (filled diamonds) are from Ref. 2.

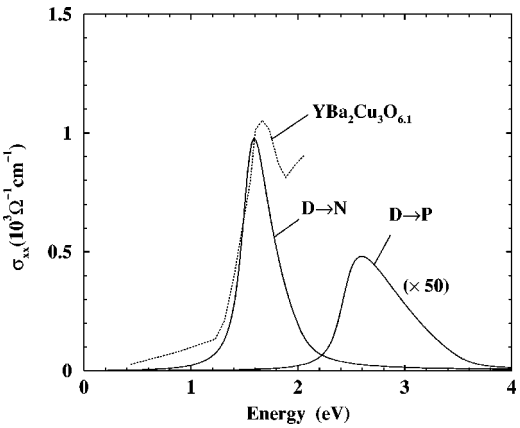

FIG. 5. The interband contributions to the optical conductivity of the three-band model ($\Sigma_2=0.1$ eV, $E_p-\mu=1.5$ eV, $m_{xx}\approx 0.4m$). The $D\rightarrow N$ ($D\rightarrow P$) contribution corresponds to the transitions between the bonding and nonbonding (antibonding) bands. For clarity the intensity of the $D\rightarrow P$ contribution is multiplied by 50. The experimental data (dotted curve) are from Ref. 3.

$\varepsilon_\infty=1$, $V_{pc}n_e=1-\delta$, and $\Sigma_1=0$ in Eq. (49)], which is expected to be $\hbar\Omega_{pl}\approx 3.4$ eV at the doping $\delta=0.2$. Such a large reduction of $\hbar\Omega_{pl}$ is ascribed primarily to the large ε_∞. This energy also depends on the mass ratio, but, for $\Sigma_1<0.1$ eV, it is practically independent of Σ_1. It can be noticed here that both Ω_{pl}^2 and $\mathrm{Re}\{\varepsilon(q_\alpha,\omega)\}$ are complicated functions of the mass ratio, though for the narrow bands (i.e., in the strong-splitting limit of the three-band model) one has the simple relation $\gamma_{\alpha\alpha}(\mathbf{k})\approx m/m_{xx}\cos\mathbf{k}\cdot\mathbf{a}_\alpha$ which leads to the linear dependance $\Omega_{pl}^2\propto m/m_{xx}$. Interestingly, the results

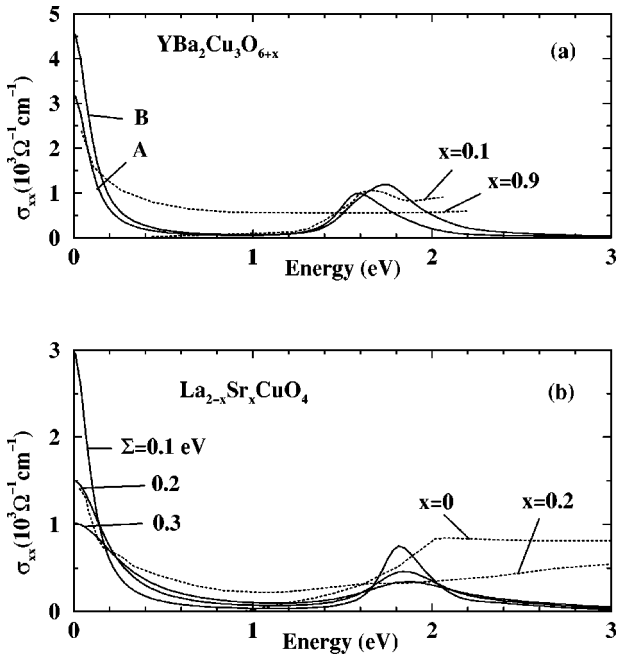

FIG. 6. Optical conductivity of the three-band model (with the fermion-boson contributions suppressed) as a function of mass ratio (a) and damping (b). For simplicity $\Sigma_1=\Sigma_2\equiv\Sigma$ is assumed. The values of the adjustable parameters are: $E_p-\mu=1.5$ eV, $\Sigma=0.1$ eV, $m_{xx}\approx m$ (curve A) and $m_{xx}\approx 0.4m$ (curve B) in (a); $E_p-\mu=1.75$ eV, $m_{xx}\approx 1.4m$ in (b). For clarity the typical measured data are also shown (dotted curves, from Refs. 2 and 3).

of the EFG analysis, when considering the different HTSC families, imply the increase of the band widths (i.e., the decrease of the mass ratio) when T_c raises (Fig. 1). The results of the present analysis, shown in Fig. 3(b), point at the same conclusion, but note that the estimated Δ_{pd}^0 ($3t_{pd}^0$ and $4.5t_{pd}^0$ for $YBa_2Cu_3O_{6.9}$ and $La_{1.8}Sr_{0.2}CuO_4$, respectively) are shifted to the higher values.

The question which remains is how Ω_{pl} depends on doping. Experiments reveal two different dependences, the hole-like (found in the underdoped and the optimally doped compounds) and the electronlike (in the overdoped materials), characterized respectively by $\partial\Omega_{pl}/\partial\delta>0$ and $\partial\Omega_{pl}/\partial\delta<0$ (see the experimental data from Ref. 2 shown in Fig. 4). For $U_d=0$, the plasma frequency (49) depends on the doping only through the variation of the chemical potential, giving rise to the $\partial\Omega_{pl}/\partial\delta<0$ behavior for the entire range of interest $0<\delta<1$, as shown in Fig. 4. In the $U_d\rightarrow\infty$ limit, however, the mass ratio m_{xx}/m and the product $m_{xx}/m\,\gamma_{xx}(\mathbf{k})$ both are dependent on δ. As mentioned above, all dependences of $m_{xx}/m\,\gamma_{xx}(\mathbf{k})$ on δ cancel out in the strong-splitting limit. In a general case one usually assumes that these ones will be finite but negligible.[13] The extensive analysis of the mean-field approximation has shown, in this respect, that the mass ratio (nearly proportional to b^{-2}) has two qualitatively different behaviors $\partial m_{xx}/\partial\delta>0$ (for the wide bands, $\Delta_{pd}^0<4t_{pd}^0$) and $\partial m_{xx}/\partial\delta<0$ (for the narrow bands, $\Delta_{pd}^0>4t_{pd}^0$).[27] Thus the only way to explain in the mean-field approximation the experimental observation at small dopings that $\partial\Omega_{pl}/\partial\delta>0$ is to consider the strong-splitting limit.[13] This is also in contrast with the conclusions of the EFG analysis which support the opposite picture of wide bands. When considering the interband terms, it is essential to stress that the expression (42) excludes the possibility of dipole-active intracell electronic collective modes (e.g., Frenkel excitons) which are present, for example, in dipolar crystals.[22]

We now turn to the structure of the incoherent interband contributions to $\mathrm{Re}\{\sigma_{\alpha\alpha}(\omega)\}$. Two of these contributions are explicitly calculated here. They are attributed to the transitions from the states on Fermi level to the states of nearly the same wave vector in the antibonding and nonbonding bands (in Fig. 5 they are labeled by $D\rightarrow P$ and $D\rightarrow N$, respectively). For the wide bands and $\Sigma_2\approx 0$ the result is a broad continuous spectrum which starts at the bare absorption edge $E_p-\mu$. However, if Σ_2 is finite, the absorption edge will be moved to lower energies, exactly as one expects for the phonon-assisted interband transitions.[23] It is important to notice here that the coherence factor $\partial R_1^{PD}(\mathbf{k}',\mathbf{k})/\partial k'_\alpha|_{\mathbf{k}'=\mathbf{k}}\propto u_{\mathbf{k}}^2-v_{\mathbf{k}}^2$ is responsible for a significant decline of the $D\rightarrow P$ contribution. In the wide band regime [see Eq. (32)] this contribution almost disappears, as can be seen in Fig. 5. This apparently means that at energies larger than 2.5 eV the spectrum $\mathrm{Re}\{\sigma_{\alpha\alpha}(\omega)\}$ is mostly associated with $\mathrm{Im}\{\varepsilon_\infty(\omega)\}$ rather than with two abovementioned interband transitions.

In the $U_d\rightarrow\infty$ limit we obtain $E_p-\mu$ to be nearly constant and of the order of t_{pd}^0, in the broad range of Δ_{pd}^0 (see Fig. 1). This qualitatively agrees with the experimental evidence that at not too large dopings the value of the absorption edge is only slightly material dependent.[2,3]

Furthermore, note that in the $U_d=0$ case Eq. (50) gives only one kind of the interband contributions among the three bands (the $D\rightarrow P$ and $D\rightarrow N$ ones). These contributions, together with the associated Drude contribution, obey some conductivity sum rules (see Fig. 6). In the strong-splitting limit of the $U_d\rightarrow\infty$ case the integrated intensities of both of these contributions are proportional to the ratio m/m_{xx} and thus to δ. They will be negligible for small dopings, pointing at the significant role of the fermion-boson excitations (associated with a new absorption edge which is of the order Δ_{pd}^0).[15] Under such conditions the latter excitations will be responsible almost for entire weight of the complete integrated intensity of the three bands. For the wide bands however, even for $U_d\rightarrow\infty$, it is expected that former two contributions will take a large share of the total integrated intensity, again with the measurable signals in the experimental spectra. In the energy range of interest (see Fig. 1) the energy Δ_{pd}^0 is larger than $E_p-\mu$, so it is natural to generalize Eq. (50) in such a manner that $\mathrm{Im}\{\varepsilon_\infty(\mathbf{Q},\omega)\}$ includes also the fermion-boson contributions. All expressions given here will be thus valid concomitantly for both considered limits.

Finally, note that although two thresholds at nearly $E_p-\mu$ and Δ_{pd}^0 are expected for $U_d\rightarrow\infty$, the measured mid-infrared absorption edge at nearly 50 meV obviously cannot be understood in the framework of the above model.

IV. CONCLUSION

In conclusion, we have presented the calculation of the dielectric function in the Emery three-band model. In the static strong-splitting limit our results reduce to the ones known from numerous previous analyses. Beyond this limit the most important results are the following. (i) For $U_d=0$, with the short-range terms in the Coulomb matrix omitted, only the incoherent electron-hole transitions appear in the interband channel of the optical conductivity. If the strong local correlations are taken into account, there is another threshold energy associated with the fermion-boson excitations. For the parameters of the considered model estimated in the EFG analysis, the ratio between these two thresholds is 2–3, in strong contrast with the ratio between the measured interband and mid-infrared thresholds, which is about 40. (ii) The magnitude of the plasma frequencies and their doping dependence measured in the overdoped compounds can be quantitatively explained in the three-band model provided that the large U_d is present. The holelike behavior $\partial\Omega_{pl}/\partial\delta>0$ found for $U_d\rightarrow\infty$ strongly contrasts the conclusions of the EFG analysis. (iii) The pp charge correlation function in the tetragonal lattices will be screened only by the corresponding short-range interactions, while the pd charge correlation function becomes dynamically screened by the long-range interactions. As a consequence, the intraband contribution to the self-energy of the A_{1g} Raman-active phonons will be small but finite, and thus sensitive to the superconducting ordering.

ACKNOWLEDGMENT

Useful discussions with Professor S. Barišić are gratefully acknowledged.

APPENDIX A: ABBREVIATIONS

The diagonalization of the Hamiltonian (6) leads to the following Bloch energies:

$$E_D(\mathbf{k})=\frac{1}{2}(E_d+E_p)-\sqrt{\frac{1}{4}(E_p-E_d)^2+t_{\mathbf{k}}^2},$$

$$E_P(\mathbf{k})=\frac{1}{2}(E_d+E_p)+\sqrt{\frac{1}{4}(E_p-E_d)^2+t_{\mathbf{k}}^2},$$

$$E_N(\mathbf{k})=E_p, \tag{A1}$$

which are attributed to the bonding, antibonding, and nonbonding bands, respectively. The associated Bloch operators are

$$L_{\mathbf{k}\sigma}^\dagger=\frac{1}{\sqrt{N}}\sum_n e^{i\mathbf{k}\cdot\mathbf{R}_n}\sum_l e^{i\mathbf{k}\cdot\mathbf{r}_l}U_{\mathbf{k}}(L,l)l_{n\sigma}^\dagger. \tag{A2}$$

The transformation-matrix elements $U_{\mathbf{k}}(L,l)$ are as follows:

$$\begin{pmatrix} U_{\mathbf{k}}(D,d) & U_{\mathbf{k}}(D,p_x) & U_{\mathbf{k}}(D,p_y)\\ U_{\mathbf{k}}(P,d) & U_{\mathbf{k}}(P,p_x) & U_{\mathbf{k}}(P,p_y)\\ U_{\mathbf{k}}(N,d) & U_{\mathbf{k}}(N,p_x) & U_{\mathbf{k}}(N,p_y)\end{pmatrix}$$
$$=\begin{pmatrix} u_{\mathbf{k}} & v_{\mathbf{k}}U_{\mathbf{k}} & v_{\mathbf{k}}V_{\mathbf{k}}\\ -v_{\mathbf{k}} & u_{\mathbf{k}}U_{\mathbf{k}} & u_{\mathbf{k}}V_{\mathbf{k}}\\ 0 & -V_{\mathbf{k}}^* & U_{\mathbf{k}}^*\end{pmatrix}. \tag{A3}$$

Here the following abbreviations are used:

$$u_{\mathbf{k}}=\frac{E_d-E_P(\mathbf{k})}{\sqrt{[E_P(\mathbf{k})-E_d]^2+t_{\mathbf{k}}^2}},$$

$$v_{\mathbf{k}}=\frac{t_{\mathbf{k}}}{\sqrt{[E_P(\mathbf{k})-E_d]^2+t_{\mathbf{k}}^2}},$$

$$U_{\mathbf{k}}=\frac{t_{x\mathbf{k}}}{t_{\mathbf{k}}},$$

$$V_{\mathbf{k}}=\frac{t_{y\mathbf{k}}}{t_{\mathbf{k}}},$$

$$t_{x\mathbf{k}}=-2\,i\,t_{pd}\sin\frac{1}{2}\mathbf{k}\cdot\mathbf{a}_1,$$

$$t_{y\mathbf{k}}=-2\,i\,t_{pd}\sin\frac{1}{2}\mathbf{k}\cdot\mathbf{a}_2,$$

$$t_{\mathbf{k}}=\sqrt{|t_{x\mathbf{k}}|^2+|t_{y\mathbf{k}}|^2}. \tag{A4}$$

APPENDIX B: SELF-CONSISTENT EQUATIONS FOR $U_D\rightarrow\infty$

At zero temperature the thermodynamic potential of the model (5) can be written in the form

$$\Omega=\sum_{\mathbf{k}\sigma}\,[E_D(\mathbf{k})-\mu]\Theta[\mu-E_D(\mathbf{k})]+N\lambda(b^2-1). \tag{B1}$$

For the doping of conducting planes δ and if the unrenormalized energy difference Δ_{pd}^0 is given, the parameters μ, λ, and b follow from three integral equations:

$$-\frac{1}{N}\frac{\partial\Omega}{\partial\mu}=1+\delta,$$

$$\frac{1}{N}\frac{\partial\Omega}{\partial\lambda}=0,$$

$$\frac{1}{N}\frac{\partial\Omega}{\partial b}=0, \tag{B2}$$

as reported earlier.[15,11,16] The boundary shape of the bonding and antibonding bands for $\delta=0.2$ is shown in Fig. 1 in the main text as a function of Δ_{pd}^0. The nonbonding band coincides with the level E_p.

APPENDIX C: CHARGE-VERTEX FUNCTIONS

In the limit of long wavelengths the leading term in the vertices $R_\nu^{LL'}(\mathbf{k}+\mathbf{q},\mathbf{k})$ can be found by using Eqs. (16), (28), (A3), and (A4). For the nearly half filled bonding band the following vertices are important:

$$R_1^{DD}(\mathbf{k}+\mathbf{q},\mathbf{k})\approx e,$$

$$[A_{1g}]R_2^{DD}(\mathbf{k}+\mathbf{q},\mathbf{k})\approx e(u_{\mathbf{k}}^2-v_{\mathbf{k}}^2),$$

$$[B_{1g}]R_3^{DD}(\mathbf{k}+\mathbf{q},\mathbf{k})\approx ev_{\mathbf{k}}^2(|U_{\mathbf{k}}|^2-|V_{\mathbf{k}}|^2), \tag{C1}$$

$$R_1^{PD}(\mathbf{k}+\mathbf{q},\mathbf{k})\approx\mathbf{q}\cdot\nabla_{\mathbf{k}'}R_1^{PD}(\mathbf{k}',\mathbf{k})|_{\mathbf{k}'=\mathbf{k}}$$

$$\approx\sum_\alpha\, q_\alpha\frac{eat_{pd}^2}{E_P(\mathbf{k})-E_D(\mathbf{k})}\,\frac{u_{\mathbf{k}}^2-v_{\mathbf{k}}^2}{t_{\mathbf{k}}}\sin\mathbf{k}\cdot\mathbf{a}_\alpha,$$

$$[A_{1g}]R_2^{PD}(\mathbf{k}+\mathbf{q},\mathbf{k})\approx-2eu_{\mathbf{k}}v_{\mathbf{k}},$$

$$[B_{1g}]R_3^{PD}(\mathbf{k}+\mathbf{q},\mathbf{k})\approx eu_{\mathbf{k}}v_{\mathbf{k}}(|U_{\mathbf{k}}|^2-|V_{\mathbf{k}}|^2), \tag{C2}$$

$$R_1^{ND}(\mathbf{k}+\mathbf{q},\mathbf{k})\approx\mathbf{q}\cdot\nabla_{\mathbf{k}'}R_1^{ND}(\mathbf{k}',\mathbf{k})|_{\mathbf{k}'=\mathbf{k}},$$

$$\approx\frac{eat_{pd}^2}{E_N(\mathbf{k})-E_D(\mathbf{k})}\,\frac{2u_{\mathbf{k}}}{t_{\mathbf{k}}}\Big(q_x\sin\frac{1}{2}\mathbf{k}\cdot\mathbf{a}_2\cos\frac{1}{2}\mathbf{k}\cdot\mathbf{a}_1$$

$$-q_y\sin\frac{1}{2}\mathbf{k}\cdot\mathbf{a}_1\cos\frac{1}{2}\mathbf{k}\cdot\mathbf{a}_2\Big),$$

$$R_2^{ND}(\mathbf{k}+\mathbf{q},\mathbf{k})\approx\mathbf{q}\cdot\nabla_{\mathbf{k}'}R_2^{ND}(\mathbf{k}',\mathbf{k})|_{\mathbf{k}'=\mathbf{k}},$$

$$[B_{2g}]R_3^{ND}(\mathbf{k}+\mathbf{q},\mathbf{k})\approx-2ev_{\mathbf{k}}U_{\mathbf{k}}V_{\mathbf{k}}. \tag{C3}$$

The corresponding irreducible representations of the D_{4h} group are also indicated.

[1] J. Orenstein, G.A. Thomas, A.J. Millis, S.L. Cooper, D.H. Rapkine, T. Timusk, L.F. Schneemeyer, and J.V. Waszczak, Phys. Rev. B **42**, 6342 (1990).

[2] S. Uchida, T. Ido, H. Takagi, T. Arima, Y. Tokura, and S. Tajima, Phys. Rev. B **43**, 7942 (1991).

[3] S.L. Cooper, D. Reznik, A. Kotz, M.A. Karlow, R. Liu, M.V. Klein, W.C. Lee, J. Giapintzakis, D.M. Ginsberg, B.W. Veal, and A.P. Paulikas, Phys. Rev. B **47**, 8233 (1993).

[4] R.M. Macfarlane, H. Rosen, and H. Seki, Solid State Commun. **63**, 831 (1987).

[5] R. Liu, C. Thomsen, W. Kress, M. Cordona, B. Gegenheimer, F.W. de Wette, J. Prade, A.D. Kulkarni, and U. Schröder, Phys. Rev. B **37**, 7971 (1988).

[6] T.P. Devereaux, D. Einzel, B. Stadlober, R. Hackl, D.H. Leach, and J.J. Neumeier, Phys. Rev. Lett. **72**, 396 (1994).

[7] A. Sacuto, R. Combescot, N. Bontemps, C.A. Müller, V. Viallet, and D. Colson, Phys. Rev. B **58**, 11 721 (1998).

[8] S. Barišić, I. Kupčić, and I. Batistić, Int. J. Mod. Phys. B **3**, 2051 (1989).

[9] C.M. Varma, Int. J. Mod. Phys. B **3**, 2083 (1989).

[10] R. Zeyher and G. Zwicknagl, Z. Phys. B **78**, 175 (1990).

[11] S. Barišić and E. Tutiš, Solid State Commun. **87**, 557 (1993).

[12] T.P. Devereaux, A. Virosztek, and A. Zawadowski, Phys. Rev. B **51**, 505 (1995).

[13] E. Tutiš, H. Nikšić, and S. Barišić, *Solid State Physics: From Quantum Mechanics to Technology*, edited by Z. Petru, J. Przystawa, and K. Repcewicz (Springer, Berlin, 1996), p. 161.

[14] V.J. Emery, Phys. Rev. Lett. **58**, 2794 (1987).

[15] G. Kotliar, P.A. Lee, and N. Read, Physica C **153-155**, 538 (1988); G. Kotliar, in *Correlated Electron Systems*, edited by V.J. Emery (World Scientific, Singapore, 1992), p. 118.

[16] I. Kupčić, S. Barišić, and E. Tutiš, J. Phys. I **6**, 2291 (1996); Phys. Rev. B **57**, 8590 (1998).

[17] I. Kupčić, Ph.D. thesis, University of Zagreb, 1998.

[18] Note that for the one-layer materials $U_{\mathbf{k}}(L,l)=U_{\mathbf{k}}(L,l)$ even for $t_\perp$ finite.

[19] S. Barišić and J. Zelenko, Solid State Commun. **74**, 367 (1990).

[20] If these off-diagonal matrix elements are omitted, the RPA equations would decouple.

[21] S. Barišić, Int. J. Mod. Phys. B **5**, 2439 (1991), and references therein.

[22] P. Županović, A. Bjeliš, and S. Barišić, Z. Phys. B **101**, 387 (1996).

[23] J.M. Ziman, *Principles of the Theory of Solids* (Cambridge University Press, Cambridge, 1979).

[24] G.D. Mahan, *Many-Particle Physics* (Plenum Press, New York, 1990).

[25] M. Opel, R. Hackl, T.P. Devereaux, A. Virosztek, A. Zawadowski, A. Erb, E. Walker, H. Berger, and L. Forró, Phys. Rev. B **60**, 9836 (1999).

[26] A.A. Abrikosov and V.M. Genkin, Zh. Éksp. Teor. Fiz. **65**, 842 (1973) [Sov. Phys. JETP **38**, 417 (1974)].

[27] E. Tutiš, Ph.D. thesis, University of Zagreb, 1994.